*M*agnetic Resonance in Solids

Electronic Journal

http://mrsej.kpfu.ru
http://mrsej.ksu.ru

* In Kazan University the Electron Paramagnetic Resonance (EPR) was discovered by Zavoisky E.K. in 1944.

Magnetic and magnetoelastic properties of non-conducting rare-earth single crystals LiLnF$_4$ (Ln = Tm, Tb, Ho, Dy) (Review)

I.V. Romanova[1,*], M.S. Tagirov[1,2]

[1]Kazan Federal University, Kremlevskaya 18, Kazan 420008, Russia

[2]Institute of Applied Research, Tatarstan Academy of Sciences,
Levobulachnaya 36a, Kazan 420111, Russia

*E-mail: romanova.irina.vladimirovna@gmail.com

We review the magnetic and magnetoelastic properties of rare earth tetrafluorides LiLnF$_4$ recently studied at Kazan Federal University in collaboration with the Laboratory of Low Temperatures, Kanazawa University, Japan.

*With great gratitude to Malkin Boris Zalmanovich in honor of his 80th birthday,
to the very best, sophisticated, sympathetic and attentive Master,
with wishes of a long life, the most intelligent students
and the great achievements in science*

1. Introduction

The study of magnetic properties of rare-earth double fluorides LiLnF$_4$ (Ln = Tm, Tb, Ho, Dy) performed over the past two decades significantly contribute to further development of the theory of magnetoelastic effects in rare-earth magnetic materials [1–3]. Their unique optical, electronic, magnetic and catalytic properties are also important for practical applications [3]. The unit cell of LiLnF$_4$ contains two magnetically equivalent sites of lanthanide Ln^{3+} ions with the S$_4$ point symmetry. The crystal structure of LiLnF$_4$ compounds is shown in Fig. 1 [4].

Magnetic properties of LiLnF$_4$ are presented in Table 1. LiTbF$_4$ and LiHoF$_4$ are dipolar Ising-like ferromagnets with magnetic moments of Tb^{3+} and Ho^{3+} ions directed along the crystallographic c-axis and Curie temperatures $T_c = 2.885$ K and 1.53 K, respectively [4]. LiDyF$_4$ is an easy-plane antiferromagnet with magnetic moments of Dy^{3+} ions arranged perpendicular to the crystal symmetry axis and an ordering temperature $T_N = 0.62$ K. LiTmF$_4$ is a Van Vleck paramagnet [4]. Magnetic dipolar interactions play the dominant role in the spontaneous low-temperature ordering of magnetic moments of Ln^{3+} ions in these compounds. Quantum phase transitions driven by transverse magnetic fields were observed in LiHoF$_4$ at temperatures below T_c [5]. LiTmF$_4$ exhibits a giant forced magnetostriction at liquid helium temperatures [6].
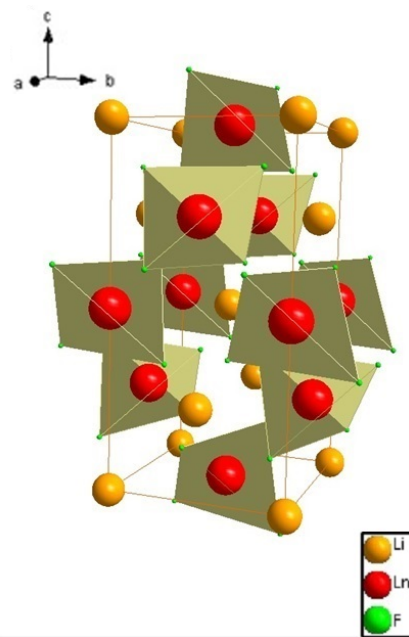

Figure 1. The crystal structure of LiLnF$_4$.

Table 1. Magnetic properties of LiLnF$_4$ compounds.

LiTmF$_4$	LiTbF$_4$	LiHoF$_4$	LiDyF$_4$
$4f^{12}$	$4f^8$	$4f^{10}$	$4f^9$
Van Vleck paramagnet	Ising-like dipole ferromagnet	Ising-like dipole ferromagnet	dipole antiferromagnet
–	$T_c = 2.89\,\mathrm{K}$	$T_c = 1.53\,\mathrm{K}$	$T_N = 0.62\,\mathrm{K}$

2. Experimental technique

Single crystals of LiDyF$_4$, LiTbF$_4$, LiTmF$_4$ and LiHoF$_4$ were grown by Dr S.L. Korableva using Bridgeman-Stockbarger method and oriented by means of X-ray diffractometer. Magnetization measurements were performed on spherical samples with known demagnetization factor. The rotation of the sample in strong magnetic fields was prevented by fixing in Stycast 1266 epoxy with an accuracy in orientation $\pm 3°$. The temperature dependences of the magnetization of single crystals in the temperature range $2-300\,\mathrm{K}$ and the magnetization curves in magnetic fields $0-5\,\mathrm{T}$ applied along and perpendicular to the c-axis were measured using dc-SQUID magnetometer MPSM-2 (Quantum Design). Angular dependences of the magnetization in the basal plane of LiDyF$_4$ and LiHoF$_4$ were measured by the inductance method with the magnetic field B up to $2\,\mathrm{T}$ applied perpendicular to the c-axis at the temperature $4.2\,\mathrm{K}$. The inductance of the coil with the sample was measured on forward and backward field sweeps by LCR-meter E7-14 using the inductance bridge circuit balanced at zero field at the frequency of $1\,\mathrm{kHz}$. The background from the empty coil was measured independently and subtracted from the total signal. The sample was glued inside the capsule and could be rotated inside the coil with an accuracy of $\pm 5°$. Magnetization curves $M(B)$ were extracted from the experimental data by integrating the field scans of the derivatives dM/dB (in arbitrary units) at various sample orientations. The obtained curves were calibrated using magnetization data for LiDyF$_4$ and LiHoF$_4$ single crystals measured with a dc-SQUID [7].

3. Theory

The Hamiltonian of a rare-earth magnetic system can be expressed by taking into account an interaction with crystal lattice with free surface, a crystal field and Zeeman energy, and interaction of a rare-earth ion with homogeneous macro- and microdeformations, magnetic dipolar and exchange interactions between ions and electron-phonon energy [8]. The Hamiltonian of a rare-earth magnetic system taking into account an interaction with a crystallographic lattice with a free surface can be written as:

$$H = \sum_{Ls} H_{L,s} + H_{\mathrm{lat}} + \sum_{Ls} \sum_{\mathbf{q}j} \sum_{pk} \frac{1}{\sqrt{N}} B_p^k(s, \mathbf{q}j) \exp(i\mathbf{q}\mathbf{R}_{Ls}) O_p^k(Ls) Q(\mathbf{q}j), \qquad (1)$$

where $H_{L,s}$ is the Hamiltonian of a rare earth ion with the radius-vector $\mathbf{R}_{L,s}$ from the sublattice sth ($s = 1,2$) in the Lth unit cell in static crystal field, H_{lat} is an energy of the crystal lattice in harmonic approximation with normal coordinates $Q(\mathbf{q}j)$ ($\mathbf{q}$ is a wave phonon vector with the frequency $\omega_{\mathbf{q}j}$, j is the number of oscillation spectrum branch), the last part in (1) represents electron-phonon energy in linear approximation on ion displacements from equilibrium positions, N is a cell number, $O_k^p(L, S)$ are linear combinations of spherical tensor operators [8] acting in the space of electron states of a rare-earth ion, $B_k^p(s, \mathbf{q}j)$ are interaction parameters determined as the derivatives of the corresponding crystal field parameters with respect to displacements of

ions [9]. Considering corrections to the energy of rare-earth ions in the second order to electron-phonon interaction at low temperature ($k_{\mathrm{B}}T \ll \hbar\omega$, k_{B} is a Boltzmann constant, ω_0 is a boundary phonon frequency) and taking into account only the mixing of electronic states with the energy difference $\Delta \ll \hbar\omega_0$, we can write the effective Hamiltonian of interaction between Ln^{3+} ions [9]:

$$\Delta H = -\frac{1}{2} \sum_{LL'ss'} (1 - \delta_{LL'}\delta_{ss'}) \sum_{pp'kk'} \Phi_{pp'}^{kk'}(ss', \mathbf{R}_{LL'}^{ss'}) O_p^k(Ls) O_{p'}^{k'}(L's'), \tag{2}$$

where

$$\mathbf{R}_{LL'}^{ss'} = \mathbf{R}_{Ls} - \mathbf{R}_{L's'}, \tag{3}$$

and

$$\Phi_{pp'}^{kk'}(ss', \mathbf{R}_{LL'}^{ss'}) = \frac{1}{N} \sum_{\mathbf{q}j} \omega_{\mathbf{q}j}^{-2} B_p^k(s, \mathbf{q}j) B_{p'}^{k'}(s', -\mathbf{q}j) \exp(i\mathbf{q}\mathbf{R}_{LL'}^{ss'}). \tag{4}$$

Two-particle interactions can be considered in a self-consistent field approximation, neglecting second-order terms with respect to deviations of the operators $O_p^k(Ls)$ from their average values $\langle O_p^k(Ls) \rangle = \langle O_p^k \rangle$ (the last equation is valid if all magnetic ions are equivalent as in case of Ln^{3+} ion in $\mathrm{LiLnF_4}$). The free energy of an elastically distorted single crystal in the presence of an applied magnetic field B can be written in the following form:

$$F = \frac{v}{2} \left[\mathbf{e}\mathbf{C'}\mathbf{e} + 2 \sum_s \mathbf{e}\mathbf{b}(r)\mathbf{w}(r) + \sum_{ss'} \mathbf{w}(r)\mathbf{a}(r,r')\mathbf{w}(r') \right] + \frac{n}{2} \sum_{pkp'k'} \langle O_p^k \rangle \lambda_{pp'}^{kk'} \langle O_{p'}^{k'} \rangle + \Delta F, \tag{5}$$

$$\Delta F = -\sum_s k_{\mathrm{B}}T \ln \mathrm{Tr} \exp(-H_{\mathrm{eff},s}/k_{\mathrm{B}}T),$$

where v is the elementary cell volume, $\mathbf{C'}$ is the tensor of "probe" elastic constants, $\mathbf{e}$ is the deformation tensor, $\mathbf{w}(r)$ is the vector of the sublattice displacement r, $b(r)$ is the relation's constants tensor of macro- and microdeformations, $a_{\alpha,\beta}(r,r')$ is the dynamic matrix of the lattice at the center of the Brillouin zone, $\lambda_{pp'}^{kk'}$ is the matrix of the relation's constants through phonon field, n is the number of equivalent magnetic sublattices ($n=2$ for $\mathrm{LiLnF_4}$), $H_{\mathrm{eff},s}$ is the effective single-ion Hamiltonian defined below:

$$H_{\mathrm{eff}} = H^{(0)} + H^{(P)}, \tag{6}$$

$$H^{(0)} = H_0 + H_{\mathrm{cf}} + H_Z, \tag{7}$$

$$H^{(P)} = \sum_{\alpha\beta} V_{\alpha\beta} e_{\alpha\beta} + \sum_{\alpha,s} V_\alpha(s) w_\alpha(s) - \sum_{pkp'k'} \lambda_{pp'}^{kk'} \langle O_p^k \rangle O_{p'}^{k'}, \tag{8}$$

The first term in (7) is the Hamiltonian of a free ion H_0, the second term is the crystal field energy, the third term is the Zeeman energy $H_Z = \mu_{\mathrm{B}}\mathbf{B}(\mathbf{L} + 2\mathbf{S})$; here μ_{B} is the Bohr magneton. First and second terms in (8) define linear interaction of rare-earth ion with homogeneous macro- and microdeformations, correspondingly. Electronic operators $V_{\alpha\beta}$ and $V_\alpha(s)$ can be presented as linear combinations of spherical tensor operators:

$$V_{\alpha\beta} = \sum_{pk} B_{p,\alpha\beta}^k O_p^k, \qquad V_\alpha(r) = \sum_{pk} D_{p,\alpha}^k(r) O_p^k. \tag{9}$$

Taking into account the translational symmetry of the lattice we can obtain from equations (2) and (3) the following equation for elements of the λ matrix in last term in (8):

$$\lambda_{pp'}^{kk'} = \frac{1}{n} \sum_{ss'} \left[\sum_{j_o} \frac{B_p^k(s, 0j_o) B_{p'}^{k'}(s', 0j_o)}{\omega_{\mathbf{0}j_o}^2} - \frac{\delta_{ss'}}{N} \sum_{\mathbf{q}j} \frac{B_p^k(s, \mathbf{q}j) B_{p'}^{k'}(s', -\mathbf{q}j)}{\omega_{\mathbf{q}j}^2} \right]. \tag{10}$$

In the first term, the summation is performed only over the optical branches of the vibrational spectrum. The single ion contribution to the free energy (5) can be written with accuracy up to second-order terms with respect to deformations characteristic of the lattice and deviations of average values of operators O_p^k from corresponding equilibrium values in a zero magnetic field (simplified equations for O_p^k are presented below). Considering operator (8) as perturbation one can rewrite $H^{(P)} = \sum_{pk} A_p^k O_p^k = A : O$, and obtain

$$\Delta F = n \left[F_0(\mathbf{B}) + \left\langle H^{(P)} \right\rangle_0 + \frac{1}{2} A : q : A \right], \tag{11}$$

where $F_0(\mathbf{B})$ is the free ion energy with Hamiltonian $H^{(0)}$, symbol $\langle ... \rangle_0$ means averaging with equilibrium density matrix $\rho = \exp(-H^{(0)}/k_\mathrm{B}T)/\mathrm{Tr}(\exp(-H^{(0)}/k_\mathrm{B}T))$. The matrix elements q equal to

$$q_{pp'}^{kk'} = \frac{1}{k_\mathrm{B}T} \left[\left\langle O_p^k \right\rangle_0 \left\langle O_{p'}^{k'} \right\rangle_0 - \sum_i \langle \psi_i | \rho O_p^k | \psi_i \rangle \langle \psi_i | O_{p'}^{k'} | \psi_i \rangle \right] +$$
$$+ \sum_{i,j \neq i} (\varepsilon_i - \varepsilon_j)^{-1} \left[\langle \psi_i | \rho O_p^k | \psi_j \rangle \langle \psi_j | O_{p'}^{k'} | \psi_i \rangle + \langle \psi_i | \rho O_{p'}^{k'} | \psi_j \rangle \langle \psi_j | O_p^k | \psi_i \rangle \right]. \tag{12}$$

Here ε_i and ψ_i are eigenvalues and eigenfunctions of operator H_{eff}. Taking into account thermodynamic equilibrium conditions $\partial F/\partial \left\langle O_p^k \right\rangle = 0$ and $\partial F/\partial w_\alpha(r) = 0$, and the designation of the convolution over the indexes p and k, introduced above, one can write the free crystal energy as

$$F = \frac{v}{2} \mathbf{e} \mathbf{C} \mathbf{e} + n F_0 - \frac{n}{2} \langle O \rangle_0 : \left[\lambda : (1 + q : \lambda)^{-1} + \frac{n}{v} \sum_{rr'} \hat{\mathbf{D}}(r) \hat{\mathbf{a}}^{-1}(r, r') \hat{\mathbf{D}}(r') \right] : \langle O \rangle_0 +$$
$$+ n \langle O \rangle_0 : (1 + \lambda : q)^{-1} : \left[\mathbf{B} - \sum_{rr'} \hat{\mathbf{b}}(r) \hat{\mathbf{a}}^{-1}(r, r') \mathbf{D}(r') \right] \mathbf{e}, \tag{13}$$

where $\hat{D}_\alpha(r) = (1 + \lambda : q)^{-1} : D_\alpha(r)$, $\mathbf{C} = \hat{\mathbf{C}}' - \sum_{rr'} \hat{\mathbf{b}}(r) \hat{\mathbf{a}}^{-1}(r, r') \hat{\mathbf{b}}(r')$ is the elastic constants tensor. The following notation for the quantities that are renormalized by the electron-deformation and electron-phonon interactions is introduced:

$$\hat{a}_{\alpha\beta}(r, r') = a_{\alpha\beta}(r, r') + \frac{n}{v} D_\alpha(r) : q : (1 + \lambda : q)^{-1} : D_\beta(r'), \tag{14}$$

$$\hat{b}_{\alpha\beta,\gamma}(r) = b_{\alpha\beta,\gamma}(r) + \frac{n}{v} B_{\alpha\beta} : q : (1 + \lambda : q)^{-1} : D_\gamma(r), \tag{15}$$

$$\hat{C}'_{\alpha\beta\gamma\delta} = C'_{\alpha\beta\gamma\delta} + \frac{n}{v} B_{\alpha\beta} : q : (1 + \lambda : q)^{-1} : B_{\gamma\delta}, \tag{16}$$

$$\hat{D}_\alpha(r) = (1 + \lambda : q)^{-1} : D_\alpha(r), \qquad \hat{B}_{\alpha\beta} = (1 + \lambda : q)^{-1} : B_{\alpha\beta}. \tag{17}$$

It should be noted that, with an accuracy of up to terms of the second order with respect to the parameters of the electron-deformation interaction, the dependence of the elastic constants on temperature and magnetic field can be represented by the expression:

$$C_{\alpha\beta\gamma\delta}(T, \mathbf{B}) = C_{\alpha\beta\gamma\delta}(T = 0, \mathbf{B} = 0) + \frac{n}{v} \hat{B}_{\alpha\beta} : q : (1 + \lambda : q)^{-1} : \hat{B}_{\gamma\delta}, \tag{18}$$

where the contributions of the magnetic subsystem are determined by the second term and the renormalized constants of coupling with macrodeformations are given by

$$\hat{B}_{p,\alpha\beta}^k = B_{p,\alpha\beta}^k - \sum_{rr'\gamma\delta} b_{\alpha\beta,\gamma}(r) a_{\gamma\delta}^{-1}(r, r') D_{p,\delta}^k(r'). \tag{19}$$

A magnetic field-induced relative change in the dimension of the crystal in the direction that is specified by the unit vector with the direction cosines n_α equals $\Delta l/l = \sum_{\alpha\beta} n_\alpha n_\beta e_{\alpha\beta}$, where components of deformation tensor are defined from minimum free energy condition (13):

$$\mathbf{e}(\mathbf{B}) = -\frac{n}{v} \left[\mathbf{SB}_{\text{eff}} : \langle O \rangle_0 |_{\mathbf{B}} - \mathbf{SB}_{\text{eff}} : \langle O \rangle_0 |_{\mathbf{B}=0} \right], \qquad (20)$$

here $B_{\text{eff}\,p,\alpha\beta}^{k} = \sum_{p'k'} [(1 + \lambda : q)^{-1}]_{pp'}^{kk'} : \hat{B}_{p',\alpha\beta}^{k'}$, $\mathbf{S} = \mathbf{C}^{-1}$ is the compliance tensor. Ion's energy levels and their magnetic moments in external magnetic field are determined by effective Hamiltonian, introduced above, where perturbation operator is:

$$H^{(P)} = \left\{ \mathbf{B}_{\text{eff}} \mathbf{e} - \langle O \rangle_0 : \left[\frac{n}{v} \sum_{rr'} \hat{\mathbf{D}}(r) \hat{\mathbf{a}}^{-1}(r,r') \hat{\mathbf{D}}(r') + \lambda : (1 + q : \lambda)^{-1} \right] \right\} : O. \qquad (21)$$

Equations defined above for elastic constants induced by magnetic field and for effective Hamiltonian of paramagnetic ion are used for calculation of LiLnF$_4$ single crystal parameters.

4. Elastic constants, magnetization and magnetostriction of LiTmF$_4$

The results that are presented below were obtained using the numerical diagonalization of the Hamiltonian of Tm^{3+} ions in the full space of states of the electronic configuration $4f^{12}$ (the number of states is 91). The Hamiltonian of the free ion was written in the standard form taking the parameters of the electrostatic, spin-orbit, and interconfigurational interactions from [10]. In the crystallographic coordinate system, the crystal field that acts on the Tm^{3+} ion in the LiTmF$_4$ crystal is determined by a set of seven parameters B_p^k:

$$H_{\text{cf}} = B_2^0 O_2^0 + B_4^0 O_4^0 + B_4^4 O_4^4 + B_4^{-4} O_4^{-4} + B_6^0 O_6^0 + B_6^4 O_6^4 + B_6^{-4} O_6^{-4}. \qquad (22)$$

The values of the crystal field parameters that were used in this work are presented in Table 2.

The calculated energy levels of the Tm^{3+} ion (see Table 3, where the sublevels of the lowest multiplet $^3H_6$ are given) agree well with experimental data. The ground state of the Tm^{3+} ions in the crystal field is the singlet $\Gamma_2(1)$, the nearest levels are the doublet $\Gamma_{34}(1)$ and the singlet $\Gamma_1(1)$ (the wave functions of different states of the electron shell $4f^{12}$ of Tm^{3+} ions are transformed according to the irreducible representations Γ_k of the S$_4$ point group). Comparison of the calculated temperature dependence of the longitudinal magnetic susceptibility with experimental data (Fig. 2) indicates that the investigated specimens of LiTmF$_4$ contain paramagnetic impurities. Their contribution to the magnetization increases considerably at temperatures lower than 10 K.

Table 2. Interaction parameters of Tm^{3+} ions with a crystal field and deformations of the B_g symmetry (in cm^{-1}).

p	k	B_p^k	p	k	$B_p^{(d)k}(B_g^1)$	$B_{\text{eff}\,p}^{k}(B_g^1)$ *	$B_p^{(d)k}(B_g^2)$	$B_{\text{eff}\,p}^{k}(B_g^2)$ *
2	0	184	2	2	1914	1571	4194	3646
4	0	−90	2	−2	1408	1337	−1030	−1169
4	4	−669	4	2	−600	−468	−1615	−1393
4	−4	−638	4	−2	1292	1141	1237	986
6	0	−4.06	6	2	−192	−164	−492	−443
6	4	−328	6	−2	−569	−480	−590	−424
6	−4	−294	6	6	−963	−858	−1375	−795
−	−	−	6	−6	−1067	−974	−1500	−910

* In a zero magnetic field at a temperature of 4.2 K

Table 3. Energy levels (in cm^{-1}) of the $^3H_6$ multiplet of the Tm^{3+} ion in a crystal LiTmF$_4$.

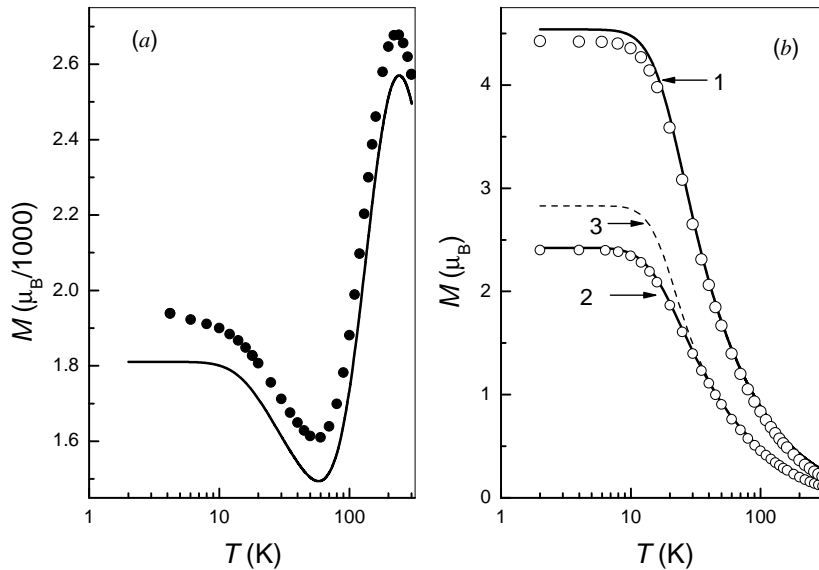| Symmetry	Experiment			Calculation
	[11]	[12]	LiYF$_4$:Tm^{3+} [13]	This work
$\Gamma_2(1)$	0	0	0	0
$\Gamma_{34}(1)$	32	–	30	31
$\Gamma_1(1)$	57	71	55	62
$\Gamma_2(2)$	–	281	275	282
$\Gamma_2(3)$	–	319	305	313
$\Gamma_1(2)$	–	363	–	362
$\Gamma_{34}(2)$	–	–	–	381
$\Gamma_{34}(3)$	–	–	–	402
$\Gamma_1(3)$	–	–	–	415
$\Gamma_2(4)$	–	–	–	430

Figure 2. Measured in [14] (symbols) and calculated (solid lines) temperature dependences of the magnetization of a LiTmF$_4$ single crystal: (a) in a magnetic field $B = 0.1$ T parallel to the c axis; (b) in magnetic fields $B = 5.5$ T (1) and 3 T (2, 3), perpendicular to the c axis and constituting an angle of 12.5 degrees with the a axis. Line 3 represents the magnetization in the 3 T field, calculated without taking into account the multipole interaction between thulium ions.

Calculations are significantly simplified if the symmetry properties of the system are taken into account. Let us introduce linear combinations of components of the deformation tensor $e(A_g^1) = e_{zz}$, $e(A_g^2) = (e_{xx} + e_{yy})/2$, $e(B_g^1) = e_{xx} - e_{yy}$, $e(B_g^2) = e_{xy}$, $e_1(E_g) = e_{xz}$, $e_2(E_g) = e_{yz}$, which transform according to the irreducible representations $\Gamma = A_g, B_g, E_g$ of the factor group symmetry of the lattice. The magnetic field that is directed along the c axis induces only totally symmetric deformations A_g, whereas field that is directed in the ab plane induces totally symmetric and rhombic deformations B_g. Corresponding microscopic deformations of the A_g and B_g symmetry are determined by three and five independent linear combinations of displacements of sublattices $w_\eta(\Gamma)$, respectively. In the basis of symmetrized deformations, the operator of the electron-deformation interaction has the following form:

$$H_{\text{el-def}} = \sum_{\Gamma v \eta} \sum_{pk} \left[B^k_{p,\eta}(\Gamma^v) e_\eta(\Gamma^v) + D^k_p, \eta(\Gamma^v) w_\eta(\Gamma^v) \right] O^k_p, \tag{23}$$

where $e_\eta(\Gamma^v)$ and $w_\eta(\Gamma^v)$ are independent variables, v and η are the number and the row of the representation Γ, respectively. Results of calculations of coupling constants in operator (23) in terms of the model of exchange charges [9] and optical piezospectroscopy of the LiTmF$_4$ crystal show that the interaction of Tm^{3+} ions with deformations of the B_g symmetry plays a dominant role. As a consequence, we may expect that dynamic deformations of the B_g symmetry make the main contribution to the multipole interaction between Tm^{3+} ions. The interaction can be represented by linear combinations of eight electronic operators: $O_2^2 = O_1$, $O_2^{-2} = O_2$, $O_4^2 = O_3$, $O_4^{-2} = O_4$, $O_6^2 = O_5$, $O_6^{-2} = O_6$, $O_6^6 = O_7$, and $O_6^{-6} = O_8$. In accordance with Eq. 9, after neglecting the dispersion of optical branches of the vibrational spectrum, we obtain the following expression for the elements of the matrix $\lambda_{i,j}$ ($i, j = 1:8$), which is determined in the space of the operators indicated:

$$\lambda_{ij} = \sum_{v=1:5} \frac{B_i(B_g^v)B_j(B_g^v)}{\omega(B_g^v)^2} - \sum_{v=1:4} \frac{B_i(A_u^v)B_j(A_u^v)}{\omega(A_u^v)^2} - \frac{1}{N} \sum_{\mathbf{q}j_a} \frac{B_i(1,\mathbf{q}j_a)B_j(1,-\mathbf{q}j_a)}{\omega^2_{\mathbf{q}j_a}}. \tag{24}$$

Multipole interaction parameters (24) were estimated using frequencies of gerade $\omega(A_u^v TO)$ and transverse ungerade $\omega(A_u^v TO)$ optical vibrations of the B_g and A_u symmetry, respectively, of the LiTmF$_4$ crystal at the center of the Brillouin zone, which were measured in [9], and coupling constants of thulium ions with corresponding vibrations which were found from the analysis of temperature and magnetic field effects in Raman spectra [9, 15], and calculations in terms of the exchange charge model. The summation over acoustic vibrations in the last term in Eq. 24 was performed in terms of the long wavelength approximation, which allow to relate the constants of the electron-phonon interaction with the electron-deformation interaction parameters (Eq. 19). The corresponding contributions to elements of the matrix $\lambda_{i,j}$ are given by (in units of 10^{-6} cm^{-1})

$$\Delta\lambda_{ij} = -\left\{ 4.48 B_i^{(d)}(B_g^1)B_j^{(d)}(B_g^1) + 2.29 \left[B_i^{(d)}(B_g^1)B_j^{(d)}(B_g^2) + B_i^{(d)}(B_g^2)B_j^{(d)}(B_g^1) \right] + \right.$$
$$\left. +1.89 B_i^{(d)}(B_g^2)B_j^{(d)}(B_g^2) \right\}. \tag{25}$$

The coupling constants with homogeneous deformations of the B_g symmetry are given in Table 2 [8]. Table 4 presents parameters of the multipole interaction, which were reduced twofold compared to calculated ones in order to match calculation results of temperature dependences

Table 4. Parameters of the multipole interaction for Tm^{3+} ions $\lambda_{i,j}$ (cm^{-1}).

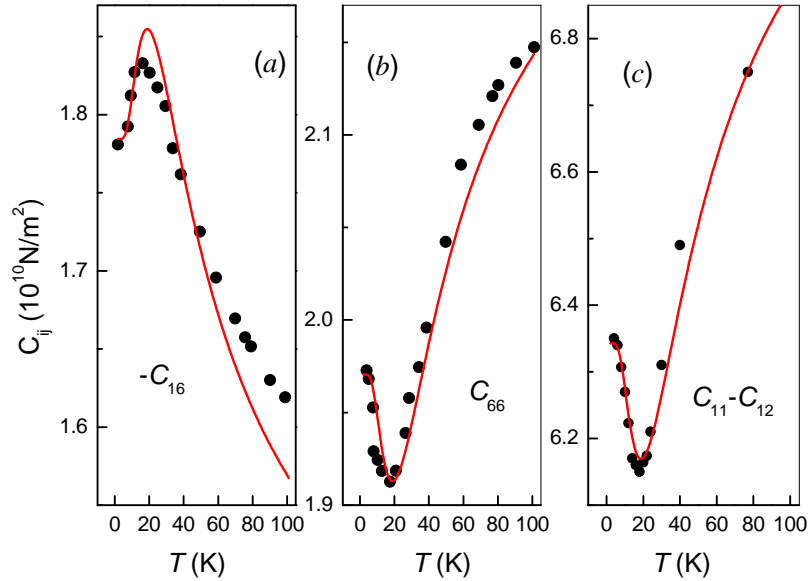| i/j	1	2	3	4	5	6	7	8
1	−32.4	−24.6	21.82	−24.7	4.58	11.92	10.13	13.48
2		28.34	−7.99	4.90	−3.21	1.582	7.23	−2.96
3			−0.90	2.06	−1.42	−0.22	−6.14	−2.20
4				−12.8	−0.80	2.15	6.34	0.512
5					−0.87	−0.52	−1.87	−0.76
6						−0.87	−2.49	−3.06
7							−2.95	−4.07
8								−2.83

Figure 3. Measured (symbols) [16] and calculated (curves) temperature dependences of the elastic constants (a) C_{16}, (b) C_{66}, and (c) $C_{11} - C_{12}$ of a single crystal LiTmF$_4$.

of the elastic constants $C_{11} - C_{12}$, C_{16}, C_{66}. Elastic constants that determine a change in the lattice energy caused by deformations of the B_g symmetry and the experimental data of [16] are shown in Fig. 3.

We note that contributions to multipole interaction parameters that are caused by the interaction of Tm^{3+} ions with acoustic vibrations (the last term in Eq. 24) and that induce long-range correlations between states of paramagnetic ions to play a dominant role. Due to renormalization (Eq. 17) the absolute values of the parameters of the effective electron-deformation interaction decrease compared to the parameters (Table 2). In calculations of magnetic field effects, magnetic dipole-dipole interactions were taken into account in terms of the self-consistent field approximation. The local magnetic field that acts on Tm^{3+} ions in the sth sublattice was given by

$$\mathbf{B}_{\mathrm{loc}}(s) = \mathbf{B} + \sum_{s'} \left[\mathbf{Q}(s, s') - \frac{4\pi}{3v} N_m \right] \mathbf{M}(s'), \tag{26}$$

where $\mathbf{M}(s')$ is the magnetic moment of the ion in the sth lattice, $\mathbf{Q}(s, s')$ are the lattice sums, which were calculated by the Ewald method; and N$_m$ is the demagnetization factor. The main attention was focused on effects that manifest themselves in magnetic fields oriented in the base plane of the lattice and that induce deformations of the B_g symmetry. The relative change in the dimension of the crystal along the magnetic field direction at ϕ angle with the crystallographic a-axis is:

$$\Delta l/l = e(A_g^2) + \frac{1}{2} \cos 2\phi \, e(B_g^1) + \sin 2\phi \, e(B_g^2), \tag{27}$$

Values of $\Delta l/l$ that were obtained upon substitution into Eq. 27 of the components of the deformation tensor calculated in accordance with Eq. 20 satisfactorily agree with the longitudinal magnetostriction data of cylindrical LiTmF$_4$ specimens with their generatrices along with directions [100] and [110] that were measured at the temperature of 4.2 K in fields with a strength of up to 3 T (see Fig. 4a).

The inverse magnetostrictive effect (a change in the crystal field as a consequence of deformations of the crystal lattice) is most clearly pronounced in splittings of non-Kramers doublets in fields with the same directions as a zero g-factor. In this case, the direct (Zeeman) interaction of a paramagnetic ion with the magnetic field splits the Kramers doublet only in the second order
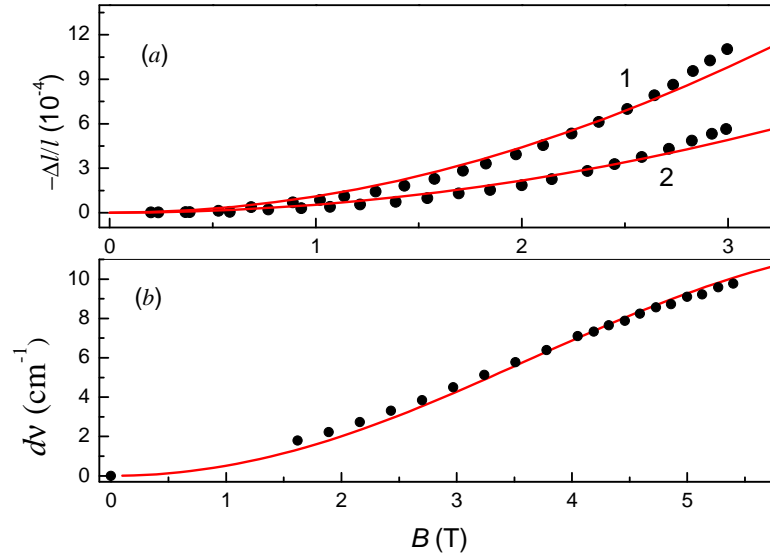
Figure 4. (a) Field dependences of the longitudinal magnetostriction of a single crystal LiTmF$_4$ at a temperature of 4.2 K in external magnetic field **B**: (1) **B** ∥ [100] and (2) **B** ∥ [110]; (b) field dependence of the splitting of doublet $\Gamma_{34}(1)$ in a magnetic field that oriented in the base plane of a single crystal LiTmF$_4$ at an angle of $\phi = 10°$ to the a axis. Results of calculations are shown by solid curves, and symbols correspond to experimental data from [4].
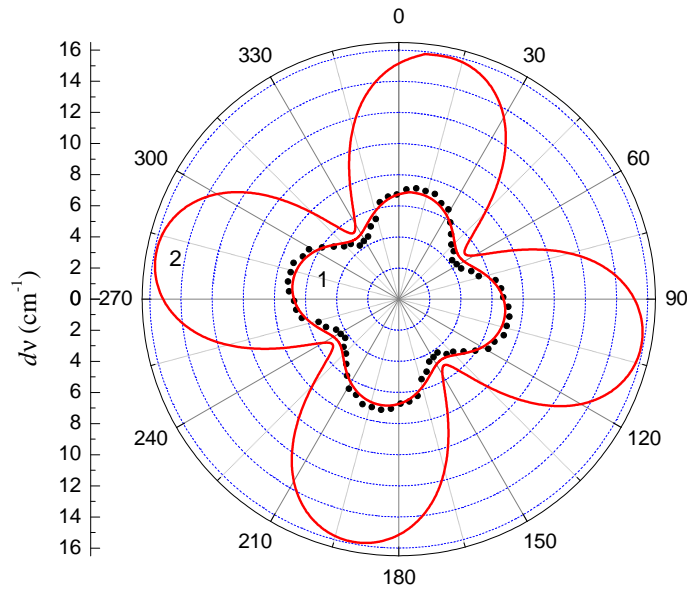

Figure 5. Measured (symbols) and calculated (curve 1) orientational dependence of the splitting of doublet $\Gamma_{34}(1)$ with an energy of 31 cm^{-1} in external magnetic field $B = 4.05$ T in the base plane of a single crystal LiTmF$_4$; $T = 4.2$ K. Curve 2 was obtained without taking into account the multipole interaction [8].

of the perturbation theory. Considerably larger splittings can occur as a consequence of field-incident changes in the lattice structure. In particular, anomalous splittings $d\nu$ of doublet $\Gamma_{34}(1)$ of thulium ions, which significantly change with the orientation of the magnetic field in the base plane of the lattice, were revealed in optical spectra of the crystal LiTmF$_4$ [17]. As can be seen from Fig. 5, the neglection of multipole interactions leads to a strong discrepancy between the results of calculations performed with the use of parameters of the electron-deformation interaction that was determined from piezospectroscopic measurements [8] and the experimental data (the calculated maximal splitting is more than two times greater than the measured splitting).
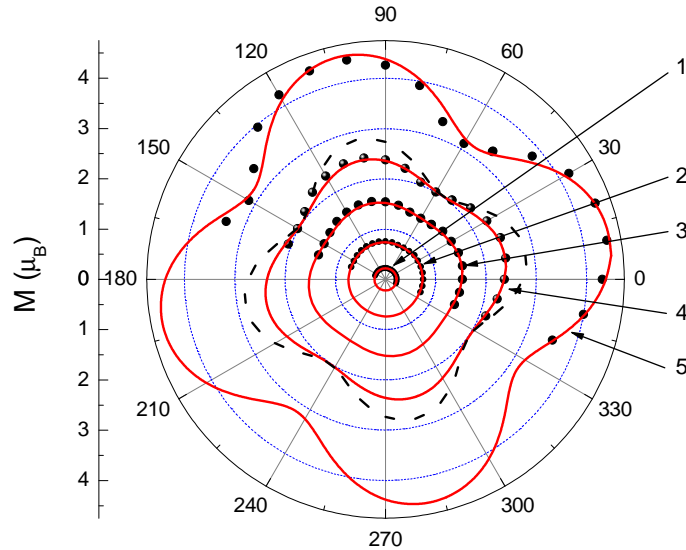
Figure 6. Measured (symbols) [18] and calculated dependences of the magnetization of a single crystal LiTmF$_4$ on the orientation of external magnetic field **B** $((1) - 0.3,\ (2) - 1.0,\ (3) - 2.0,$ $(4) - 3.0,$ and $(5) - 5.5$ T) in the base plane of the lattice; $T = 4.2$ K. The dashed curve shows the results of the calculation ($B = 3$ T) that was performed without taking into account the multipole interaction.

However, if the operator (21) which contains renormalized effective constants of the electron-deformation interaction is used, the calculated field Fig. 4b and orientational Fig. 6 dependences of splitting $d\nu$ of doublet $\Gamma_{34}(1)$ agree well with the measured dependences.

Changes in the electronic structure of paramagnetic ions that are caused by lattice deformations in a magnetic field give rise to corresponding additional contributions to the field-induced magnetization. As in the case of the splitting of doublet $\Gamma_{34}(1)$ considered above, we obtained overestimated values of magnetic moments of thulium ions in magnetic fields that were perpendicular to the c axis and the strength of which was above 1 T (Fig. 4b) without taking into account multipole interactions. The measured temperature, field, and orientational dependences of the magnetization is reproduced well only in calculations performed using parameters of the electron-deformation and multipole interactions that are the same to used ones in the above-considered calculations of elastic constants, magnetostriction, and spectrum of thulium ions.

5. Magnetic properties of the ising dipole ferromagnet LiTbF$_4$

In the crystal field the fundamental term $^7F_6$ of the Tb^{3+} ion is split into seven sublevels corresponding to the irreducible representations Γ_1 (three singlets), Γ_2 (four singlets), and Γ_{34} (three doublets) of point-group symmetry S$_4$. The ground state of the Tb^{3+} ion is characterized by a quasi-doublet consisting of two singlets ($k = 1, 2$) with the initial splitting $\delta \approx 1\,\mathrm{cm}^{-1}$; in this case, the Δ energy of the nearest neighbour excited state (the Γ_{34} doublet) is of the order of $100\,\mathrm{cm}^{-1}$ [3]. At low temperatures ($k_\mathrm{B}T \ll \Delta$) only the fundamental quasi-doublet is virtually filled. Since sublevels of the Γ_2 symmetry are mixed only with the component of the external magnetic field **B**$_0$ that is oriented along the [001] axis of the crystal lattice (we used the crystal system of coordinates in which the z-axis is aligned parallel to the c axis), the magnetic properties of the LiTbF$_4$ single crystal can be considered within the model of an Ising three-dimensional magnet in a transverse magnetic field whose role is played by the initial splitting δ of the quasi-doublet. The Hamiltonian of the system can be represented in terms of the operators of the effective spin moment components S_α^i of the i-th Tb^{3+} ion ($S = 1/2$) in the following form:

$$H_{\text{eff}} = -\frac{1}{2} \sum_{i,j} \left[\frac{(g_\parallel \mu_B)^2}{v} K_{ij} + J_{ij} \right] S_z^i S_z^j - \sum_i (\delta S_x^i + g_\parallel \mu_B B_z S_z^i). \tag{28}$$

Here the first sum corresponds to the pair magnetic dipole-dipole and exchange interactions, $K_{ij} = v(3z_{ij}^2 - r_{ij}^2)/r_{ij}^5$, $v = a^2 c/2$ is the volume of the unit cell, and $\mathbf{r}_{ij}$ is the vector connecting two Tb^{3+} ions. The intrinsic magnetic moment of the Tb^{3+} ions is characterized by only the z component oriented along the symmetry axis of the crystal lattice. By virtue of the large effective g factor ($g_\parallel = 2g_L = 17.85$ [10], where $g_L = 3/2$ is the Landé splitting factor and J is the total angular momentum of the ion), the magnetic dipole-dipole interaction plays a dominant role in magnetic ordering. Since the magnetic dipole-dipole interaction is a long-range interaction, the calculation of the low-temperature magnetic characteristics of the $LiTbF_4$ single crystal within the self-consistent field approximation is justified.

6. Exchange interaction in $LiTbF_4$ single crystal

In the self-consistent field approximation the local magnetic field acting on Tb^{3+} paramagnetic ions in a single-crystal sample along the [001] direction can be represented as the sum of the external magnetic field $\mathbf{B}_{0z}$, the molecular field $B_M = \lambda M$, and the demagnetizing field $\mathbf{B}_D = -D\mathbf{M}$, where $\mathbf{M}$ is the magnetization of the sample, D is the demagnetizing factor (for a spherical sample, $D = 4\pi/3$), $\lambda = \lambda_D + \lambda_J$ is the molecular field constant, and $\lambda_D = \sum_j D_{ij}/2 = 4\pi/3 \cdot 1.3965$ is the Lorentz field constant obtained by summation over the lattice (in our case, the unit cell contains two paramagnetic ions). The exchange field constant $\lambda_J = v \sum_j J_{ij}/2(g_\parallel \mu_B)^2$ is determined by the exchange interaction between the nearest neighbour ions [19]. In particular, based on analyzing the data on quasi-elastic neutron scattering by a $LiTbF_4$ crystal, estimated the exchange integrals for interactions of terbium ions with the nearest neighbour ions (for four ions located at a distance of 0.375 nm, $J_1 = -0.3624 \pm 0.125$ cm^{-1}) and with the next-to-nearest neighbour ions (for ions located at a distance of 0.518 nm, $J_2 = 0.07 \pm 0.14$ cm^{-1}). In this case the molecular field constant is estimated to be $\lambda = 5.23 \pm 0.56$. In the self-consistent field approximation the molecular field constant λ can be related to the observed temperature of magnetic ordering through the relationship

$$1 = \lambda \frac{(g_\parallel \mu_B)^2}{v\delta} \text{th} \frac{\delta}{2k_B T_c}. \tag{29}$$

By substituting $\delta = 1.1$ cm^{-1} and $T_c = 2.88$ K into relationship Eq. 29, we can estimate the molecular field constant from below: $\lambda > 4.32$. For the paramagnetic phase at sufficiently low temperatures ($T_c < T < \Delta/k_B$) and in weak magnetic fields $B_{0z} \ll \delta/(g_\parallel \mu_B) \approx 0.1$ T, the magnetization along axis c of the lattice can be represented by the expression Eq. 30

$$M_z = B_{0z} \left[\lambda \left(\frac{\text{th}(\delta/2k_B T_c)}{\text{th}(\delta/2k_B T)} - 1 \right) + D \right]^{-1}. \tag{30}$$

In the case when the dipole-dipole interaction between paramagnetic ions dominates in the crystal, a decrease in temperature below the Curie point leads to the formation of domains with a zero demagnetizing factor (i.e., long thin cylinders with a generatrix along the magnetization axis are formed) [19]. Note that the total magnetic moment of the crystal $\mathbf{M}V$ (V is the crystal volume) remains zero. In a weak external magnetic field, the domains are partially reoriented; as a result, the demagnetizing field B_{Dz} completely compensates for the external magnetic field B_{0z} and the magnetization of the crystal is equal to the limiting magnetization defined by expression Eq. 30; i.e., $M_z = B_{0z}/D$ at $T \to T_c$ and under the condition $B_{0z} < M_0/D = B_c$. Here, M_0 is the spontaneous magnetization at a specified temperature of the sample, which satisfies the
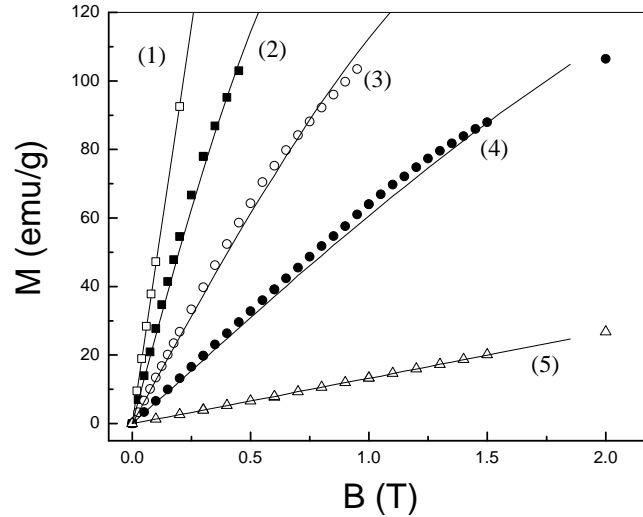
Figure 7. Magnetization of the LiTbF$_4$ single crystal as a function of the external magnetic field strength ($\mathbf{M} \parallel \mathbf{B}_0 \parallel c$) at temperatures of $(1) - 2$, $(2) - 5$, $(3) - 10$, $(4) - 20$, and $(5) - 77$ K. Symbols indicate the experimental data, and solid lines represent the results of calculations.
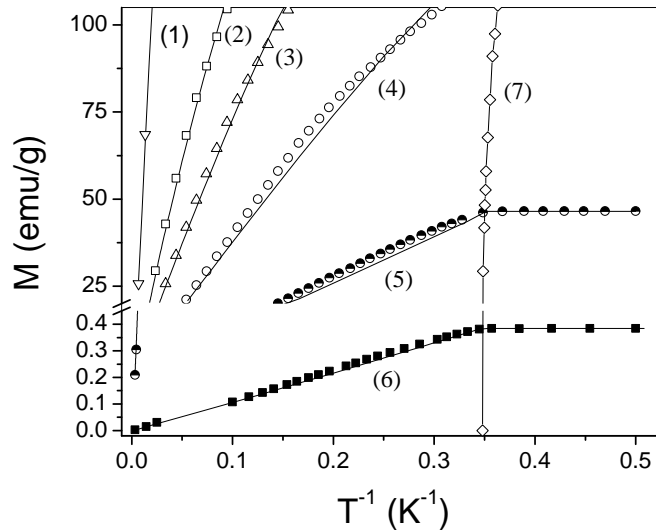

Figure 8. Temperature dependences of the magnetization of the LiTbF$_4$ single crystal in the magnetic field $\mathbf{B}_0 \parallel c$. Magnetic field strength $\mathbf{B}_0$: $(1) - 5.0$, $(2) - 1.0$, $(3) - 0.6$, $(4) - 0.3$, $(5) - 0.1$, and $(6) - 9 \cdot 10^{-4}$ T. Symbols indicate the experimental data, and solid lines represent the results of calculations using (32). Spontaneous magnetization is taken from [4].

following relationship

$$\frac{\delta}{[\delta^2 + (g_{\parallel}\mu_{\mathrm{B}}\lambda M_0)]^{1/2}} \frac{\mathrm{th}[\delta^2 + (g_{\parallel}\mu_{\mathrm{B}}\lambda M_0)]^{1/2}/2k_{\mathrm{B}}T}{\mathrm{th}(\delta/2k_{\mathrm{B}}T_c)} = 1. \tag{31}$$

Thus, the dependence of the induced magnetization on the external magnetic field is linear at $T < T_c$ and the saturation of magnetization occurs upon reorientation of all the domains involved. As can be seen from Fig. 7, the magnetization measured at a temperature of 2 K is a linear function of the external magnetic field (straight line 1); in this case, the demagnetizing factor is estimated to be $D = 3.91 \pm 0.2$.

The experimental temperature dependence of the magnetization measured in a very weak magnetic field is shown in Fig. 8 (curve 6). The observed increase in the magnetization with a decrease in the temperature is adequately described by expression Eq. 30 with the molecular field constant $\lambda_{\mathrm{exp}} = 4.525$ and demagnetizing factor $D = 4.11$, which correspond to the hori-

zontal portion of the curve M_z. The solid lines in Fig. 7 and Fig. 8 (except for curve 7 in Fig. 8) represent the results of our calculations with the same molecular field constant $\lambda_{\exp} = 4.525$. Therefore, the ratio of the energy of exchange (antiferromagnetic) interaction between the nearest neighbour ions to the energy of their magnetic dipole-dipole interaction can reach a value of -0.42. The derivative $dM_z(T, B_{0z})/dT$ has a discontinuity at the point of intersection of the curves $M_z(T)$ and $M_0(T)$, which represent the temperature dependences of the induced magnetization and the spontaneous magnetization, respectively. Curve 7 in Fig. 8 depicts the temperature dependence of the spontaneous magnetization of the LiTbF$_4$ crystal according to the magnetic neutron scattering data obtained in [4]. It can be seen from the temperature dependences of the magnetization measured in magnetic fields of $9 \cdot 10^{-4}$ and $0.1\,\mathrm{T}$ (Fig. 8) that, in actual practice, similar information on the spontaneous magnetization of a dipole ferromagnet can be obtained from significantly simpler measurements of the induced magnetization.

7. Parameters of the crystal field in LiTbF$_4$ single crystal

For high temperatures (at which the populations of the excited Stark sublevels of the fundamental term $^7F_6$ for the Tb^{3+} ions should be taken into account) and strong magnetic fields with considerable mixing of the wave functions of the fundamental quasi-doublet and excited sublevels, the magnetization can be calculated as a function of the temperature and the local magnetic field $\mathbf{B}_{\mathrm{loc}} = \mathbf{B}_0 + \mathbf{B}_M + \mathbf{B}_D$ in the framework of the single-ion approximation; that is,

$$\mathbf{M} = \frac{2g_L\mu_{\mathrm{B}}}{\nu} \frac{\mathrm{Sp}[\mathbf{J}\exp(-H/k_{\mathrm{B}}T)]}{\mathrm{Sp}[\exp(-H/k_{\mathrm{B}}T)]}. \tag{32}$$

Here, H is the single-ion Hamiltonian operator involving the energy of the rare-earth ion in the crystal field and the energy of the Zeeman interaction:

$$H = H_{\mathrm{cf}} + g_L\mu_{\mathrm{B}}\mathbf{J}\mathbf{B}_{\mathrm{loc}}. \tag{33}$$

The dependence of the magnetization on the external magnetic field $\mathbf{B}_0$ can be obtained from relationship Eq. 32 by comparing $M(B_{\mathrm{loc}})$ and $\mathbf{B}_0 = \mathbf{B}_{\mathrm{loc}} - (\lambda - D)\mathbf{M}(\mathbf{B}_{\mathrm{loc}})$. It should be noted that there is a wide scatter of the data available in the literature on the crystal field parameters for terbium ions in isostructural crystals LiTbF$_4$ and LiYF$_4$: Tb^{3+} (Tb^{3+} ions substitute for Y^{3+} ions) [19]. Since the form of Hamiltonian Eq. 22 remains unchanged upon an arbitrary rotation of the coordinate system about the [001] quantization axis and, in particular, the x and y axes can be chosen in the basal plane of the crystal lattice in such a way that one of the four parameters $B_4^{\pm 4}$, $B_6^{\pm 4}$ becomes zero. Information regarding the g factors and relative energies of the sublevels of the fundamental term of the paramagnetic ion, which is derived from investigations into the linear magnetic susceptibility and optical spectra, makes it possible to determine only six of the seven parameters B_p^k involved in the Hamiltonian operator (28). With the aim of determining the parameters of the crystal field in LiLnF$_4$ crystals (Ln = Tb, Dy, Ho, Er, and Yb), Nevald and Hansen [20] studied the nonlinear magnetic susceptibility anisotropy in the basal plane of the crystal system and analyzed the results of magnetic measurements in terms of the single-ion Hamiltonian Eq. 33. However, the magnetic anisotropy of concentrated rare-earth paramagnets at low temperatures is characterized by a substantial contribution of the magnetoelastic interaction. Therefore, in the general case, the Hamiltonian operator Eq. 33 should contain terms accounting for the interaction between the rare-earth ion and the lattice strain induced by the magnetic field. In LiTbF$_4$ crystals the magnetoelastic interaction is suppressed by virtue of the large difference between the energy of the ground state (quasi-doublet) and the energy of the nearest neighbour excited states [6]. For the same reason, the Van Vleck paramagnetic susceptibility in the ground state is small and its anisotropy in the basal
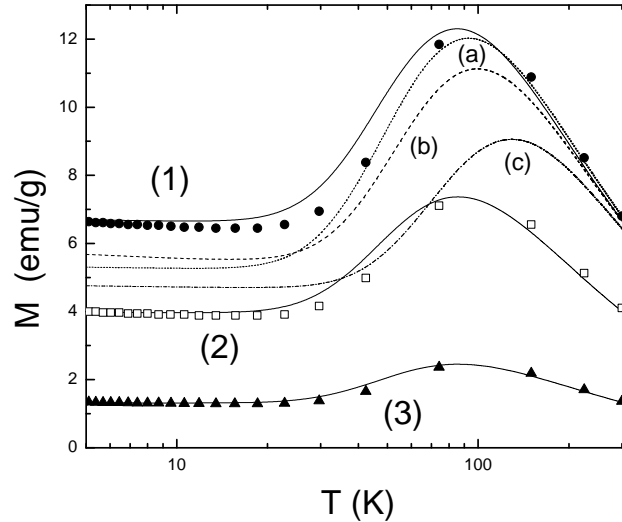
Figure 9. Temperature dependences of the magnetization of the LiTbF$_4$ single crystal in the magnetic field $\mathbf{B}_0 \perp c$. Magnetic field strength $\mathbf{B}_0$: $(1) - 5$, $(2) - 3$, and $(3) - 1$ T. Symbols indicate the experimental data. Theoretical temperature dependences of the magnetization is calculated using the crystal field parameters obtained in this work (solid lines) and (at $B_0 = 5$ T) the parameters taken from (a) [20] (dotted line), (b) [3] (dashed line), and (c) [19] (dot-dashed line).

plane is virtually absent. Nonetheless, the transverse magnetization can change significantly with an increase in the temperature and upon filling of excited non-Kramers doublet states, which are characterized by a considerable mixing with closely spaced singlet states in the magnetic field $\mathbf{B}_0 \perp c$. Figure 9 presents the results of our measurements of the transverse magnetization of the LiTbF$_4$ single crystal over a wide temperature range in magnetic fields with inductions of 1, 3, and 5 T. Owing to the very large difference (up to two orders of magnitude in a magnetic field with an induction of 1 T) between the longitudinal and transverse magnetic susceptibilities of the terbium ions, even an insignificant deviation of the external magnetic field direction in the basal plane may introduce large errors into the results of the magnetic measurements. We compared the results of magnetic measurements at different orientations of the external magnetic field with respect to the symmetry axis of the crystal lattice and estimated the error $\delta\phi < 0.8°$ in the orientation of the magnetic field with respect to the (x, y) plane in the experiments, the results of which are presented in Fig. 9. An insignificant increase in the magnetization with an increase in temperature from 3 to 20 K is caused by a decrease in the contribution from the longitudinal component of the magnetic moment of the terbium ions (Fig. 8). With a further increase in temperature, the transverse magnetization increases substantially and reaches a maximum at a temperatures of 80–90 K. The magnetization $\mathbf{M} \parallel \mathbf{B}_0 \perp c$ was calculated according to relationships Eq. 32 and Eq. 33.

The results of these calculations are presented in (Fig. 9). The non-monotonic behaviour of the temperature dependence of the transverse magnetization can be explained by the anomalously large field-induced magnetic moment at the lower sublevel of the non-Kramers doublet Γ_{34} (nearest to the ground state) with an energy of $108\,\text{cm}^{-1}$. As can be seen from (Fig. 9), the results of magnetization calculations with the use of the crystal field parameters available in the literature (see Table 5) differ significantly from the results of magnetization measurements.

The small correction to the crystal field parameters calculated in [19] within the model of exchange charges made it possible to describe adequately both the energy of Stark sublevels of the $^7F_6$ term (in particular, we calculated the splitting of the fundamental quasi-doublet $\delta = 1.09\,\text{cm}^{-1}$, the splitting factor $g_{\parallel} = 17.90$, and the energy of the nearest neighbour doublet

Table 5. Crystal field parameters B_p^k (cm^{-1}), acting on Tb^{3+} in LiTbF$_4$ and LiYF$_4$:Tb^{3+} single crystals.

	[21]	[16]	[22]	[21]	LiYF$_4$:Tb^{3+}[23]	This work
B_2^0	237	237	227.5	222.5	200	200
B_4^0	−54.1	−54.1	−121.2	−95	−100	−100.5
B_6^0	4	4	−30.3	0.25	−3.56	−2
B_4^4	−1130	−854.2	−946.5	−1171	−1103	−694
B_4^{-4}	0	−739	0	0	0	−829
B_6^4	−522	−477	−84.5	−534	−529	−435
B_6^{-4}	−201	−291	±93.8	−427	0	−283

$\delta = 1.09$ cm^{-1}), the temperature and field dependences of the magnetization. The results of our calculations are shown by solid lines in Figs. 7-9. In conclusion, we note that the results obtained in the present work can be useful for the systematization of information on the exchange interaction and crystal field parameters for crystals of double rare-earth fluorides.

To determine ratios of the parameters $B_4^{\pm 4}$, $B_6^{\pm 4}$, we analyzed presented in [24] dependences of the longitudinal magnetization in LiTbF$_4$ on the external pulsed magnetic fields applied to the oriented samples (rectangular rods with dimensions of $1.5 \times 1.5 \times 2.5$ mm^3) in the ab-plane along the [100] and [110] directions (coinciding with the long edge of a rod) at the temperature 1.4 K. The magnetic field varied from zero up to 50 T during 20 μs, and we calculated the magnetization assuming the adiabatic process similarly to the authors of [24]. Changes of the temperature ΔT of the magnetic subsystem induced by the increase of the field with steps ΔB were calculated using the following expression

$$\Delta T = -T \frac{\langle H_{\text{eff}}(\mathbf{B})\mathbf{m} \rangle - \langle H_{\text{eff}}(\mathbf{B}) \rangle \langle \mathbf{m} \rangle}{\langle H_{\text{eff}}(\mathbf{B})^2 \rangle - \langle H_{\text{eff}}(\mathbf{B}) \rangle^2} \Delta \mathbf{B}. \tag{34}$$

There are two terbium ions, Tb1 and Tb2, with coordinates $\mathbf{r}$(Tb1) $= (0, 0, c/2)$, $\mathbf{r}$(Tb2) $= (0, a/2, -c/4)$ in the unit cell. According to neutron scattering data [25] at 100 K, the lattice constants of LiTbF$_4$ equal $a = 0.5181$ nm, $c = 1.0873$ nm. In the magnetically ordered state, the local field at the terbium ion Tbs ($s = 1, 2$) is written as follows

$$B_{\text{loc},\alpha}(\text{Tb}s) = B_\alpha + \sum_\beta \left[\sum_{s'=1,2} Q_{\alpha\beta}(\text{Tb}s, \text{Tb}s') + 2\frac{4\pi}{3v}(\lambda_{is} - N_\alpha)\delta_{\alpha\beta} \right] m_\beta(\text{Tb}). \tag{35}$$

Here the demagnetizing factors of the rods are $N_x = N_y = 0.68$ [22], $N_z = 0$ (for the domains in the system with the dominant dipole-dipole interactions), the lattice sums $Q_{\text{Tb}s,\text{Tb}s}(xx) = Q_{\text{Tb}s,\text{Tb}s}(yy) = 1.18053$, $Q_{\text{Tb}s,\text{Tb}s}(zz) = 0.63894$, $Q_{\text{Tb1},\text{Tb2}}(xx) = Q_{\text{Tb1},\text{Tb2}}(yy) = 0.41738$, $Q_{\text{Tb1},\text{Tb2}}(zz) = 2.16525$ (in units of $4\pi/3v$) have been computed by the Ewald method, the value of the isotropic exchange (antiferromagnetic) field constant $\lambda = -0.316$ have been determined previously in [26]. The small initial external field of 0.01 T has been introduced to account for the ordering of magnetic moments along the c-axis. With the increasing magnetic field normal to the magnetic easy axis [001], the gap between the lower sublevel of the first excited Γ_{34} state and the ground quasi-doublet quickly diminishes (see Inset (a) in Figure 10), and the peaks in the differential magnetic susceptibility are observed at the anticrossing point. As an example, evolutions of the spontaneous magnetic moment with the increasing transversal external field and of the induced moment along the field are shown in Inset (b) in Fig. 10. As it is seen in Fig. 10, the differential susceptibilities computed with our set of the crystal field parameters match
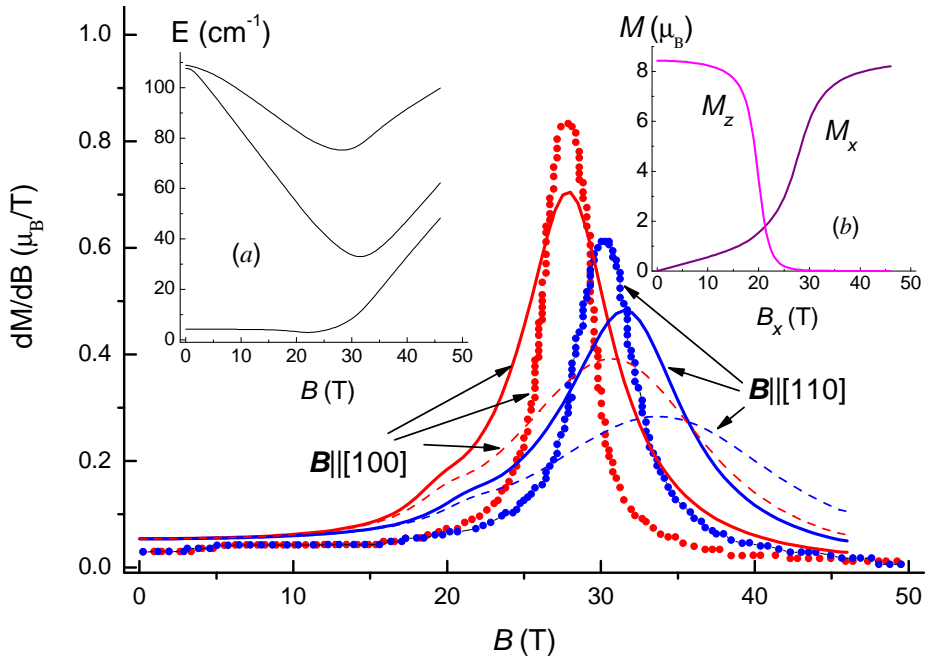
Figure 10. Differential magnetic susceptibilities of LiTbF$_4$ single crystals in magnetic fields **B** ∥ [100] and **B** ∥ [110] (in red and blue, respectively), $T = 1.4$ K. Symbols – experimental data digitized from Ref. [26], solid and dashed curves represent the results of calculations carried out with or without taking into account the magnetoelastic interactions, respectively. Inset (a) – calculated energies of the three lower sublevels of the $^7F_6$ multiplet relative to the ground state vs. the magnetic field **B** ∥ [110]. Inset (b) – calculated magnetization components along (induced moment M_x) and normal (spontaneous moment M_z) to the external field **B** ∥ [100] vs. the field intensity.

satisfactorily experimental data. However, the widths of the calculated peaks are much broader than the measured ones. It is evident that more elaborated study of the quantum phase transition in LiTbF$_4$ in the transversal magnetic fields beyond the mean field approximation is necessary. A comparison of the solid and dashed curves in Fig. 10 shows that magnetoelastic interactions contribute substantially into the magnetization if the magnetic field is strong enough.

8. Magnetization and magnetostriction in a single crystal of LiHoF$_4$

The LiHoF$_4$ crystal is considered in many works as a model Ising dipole ferromagnet with an easy magnetization axis that coincides in direction with the crystallographic axis c. The literature presents several different sets of parameters of the crystal field for holmium ions in LiHoF$_4$ crystals found from the analysis of optical spectra (see Table 6).

Table 6. Crystal field parameters B_p^k (cm^{-1}), acting on Ho^{3+} in LiHoF$_4$ single crystals.

	[27]	[28]	[29]	This work
B_2^0	219.7	190.35	190	200.35
B_4^0	−87.3	−78.25	−78	−84.25
B_6^0	−3.55	−3.25	−3.2	−3.5
B_4^4	−710	−657.2	869	−667.24
B_4^{-4}	−612	−568.6	0	−578.63
B_6^4	−387	−364	427	−364.04
B_6^{-4}	−253.7	−222.3	105	−222.3

Table 7. Experimental and calculated energy levels of holmium ions in $LiHoF_4$.

$^{2S+1}L_J$	Γ	Experimental	Calculation
	34	0	0
	2	7.4	7.35
	2	23.1	18.88
	1	49	49.68
	1	61	58.72
	34	72.1–78	68.88
$^5I_8$	1		202.14
	34		259.12
	1		259.23
	2		267.2
	34		280.86
	1		282.47
	2		295.85

Table 8. The parameters of the interaction of Ho^{3+} ions with deformations of A_g, B_g symmetry used in the work (cm^{-1}).

p	k	$B_p^{(d)k}(A_g^1)$	$B_p^k(A_g^2)$	p	k	$B_p^{(d)k}(B_g^1)$	$B_p^k(B_g^2)$
2	0	-398.2	−1692.9	2	2	2045	4114
4	0	308	1100	2	−2	2305	−886
4	4	5061.3	5280.4	4	2	−854	−1554
4	−4	3761.8	5602.5	4	−2	1449	1423
6	0	235.4	-166.1	6	2	135	−528
6	4	1930.8	3194.9	6	−2	-427	−523
6	−4	950.8	3009.7	6	6	−606	−927
				6	−6	−691	−1046

The Stark structure of energy levels is shown in Table 7 in comparison with the experimentally measured values [18] and calculated by diagonalization the above Hamiltonian Eq. 22 on a complete basis of 1001 states. The basic term $^5I_8$ of the electron shell $4f^{10}$ is split into 13 levels: 9 singlets and 4 doublets. The ground state is the non-Kramers doublet Γ_{34} and the two overlying excited states are singlets Γ_2. The parameters of the Hamiltonian of free Ho^{3+} ions used in this work are presented in [30]. From Table 7 it can be seen that good agreement is obtained between the experimental data and the calculation.

The magnetostriction in a $LiHoF_4$ single crystal was measured in Ref. [2]. The change in the dimensions of the single crystal was measured along the direction of the crystallographic axis c, and the external magnetic field was applied in the basal plane ab. When calculating the magnetostriction, the refined parameters of the electron-deformation interaction were used. The values of the parameters of the electron-deformation interaction used in this work are listed in Table 8.

The changes in the crystal size $\Delta l/l = \sum_{\alpha\beta} n_\alpha n_\beta e_{\alpha\beta}$ calculated using the above crystal field parameters and the electron-deformation interaction parameters are shown in Fig. 11. It can be seen that the qualitative agreement is very good, but at 1.6 K the calculation gives underestimated values close to the values at 1.8 K.

The field dependences of the magnetostriction were calculated with the refined crystal field parameters and the parameters of the electron-deformation interaction along the direction of the external magnetic field given by the direction cosines n_α. The results are in qualitative agreement with the measurement data (see Fig. 12).

The results of calculations of the magnetization of a LiHoF$_4$ single crystal as a function of the magnetic field directed along the a and c axes at different temperatures and the angular dependence of the magnetization upon rotation of the field in the basal plane are compared with experimental data in Figs. 13–15. The field and temperature dependences of the magnetization
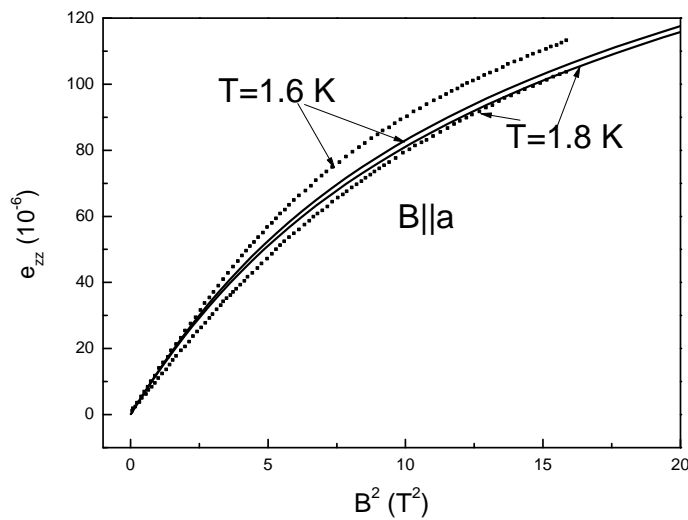

Figure 11. Magnetostriction in a single crystal of LiHoF$_4$ along the crystallographic c axis in a magnetic field applied in the ab plane at different temperatures, depending on the magnitude of the square of the external magnetic field. Points – experimental data [2], solid lines – calculation.
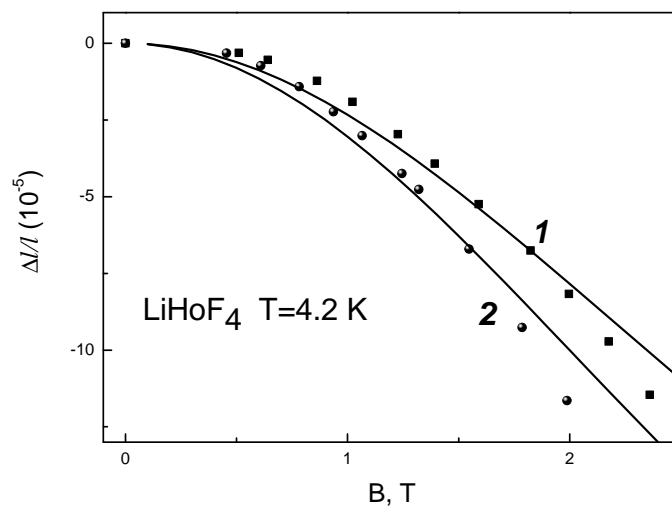

Figure 12. Field dependences at a temperature of 4.2 K of longitudinal magnetostriction in an external magnetic field **B** ($1 - $**B** $\parallel [110], 2 - $**B** $\parallel [210]$) of a single crystal of LiHoF$_4$. The results of the calculations are represented by lines, the symbols correspond to the experimental data. (Experimental data were obtained by V.I. Krotov, personal communication.)
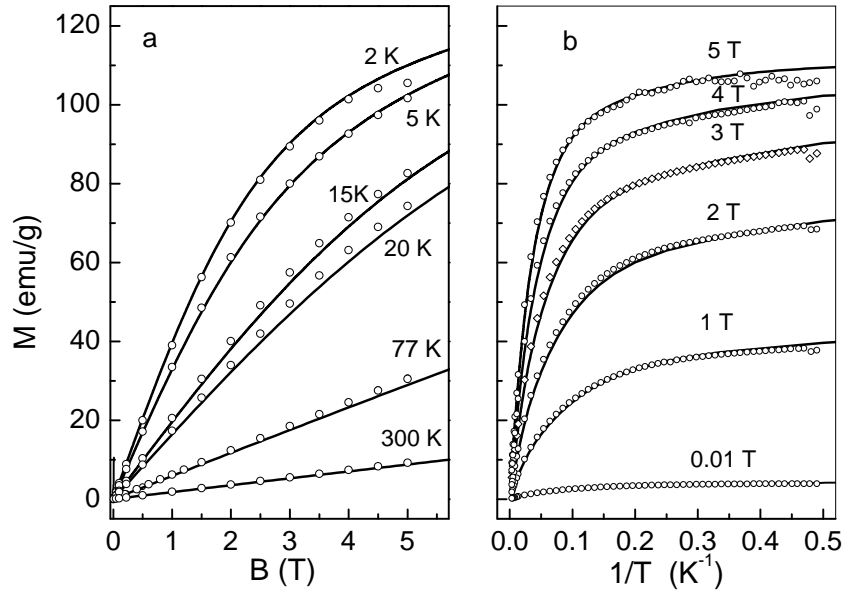
Figure 13. Field (a) and temperature (b) dependences of the magnetization along the a axis of a single crystal of a LiHoF$_4$. Solid lines are theoretical results, symbols are experimental data [6].

Figure 14. Field (a) and temperature (b) dependences of the magnetization along the c axis of a single crystal of a LiHoF$_4$. Solid lines are theoretical results, symbols are experimental data [6].
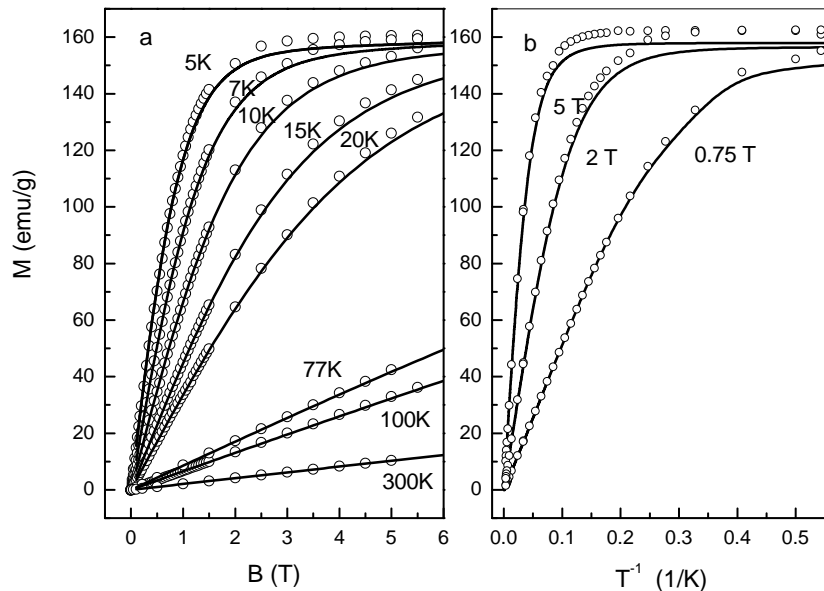
of a LiHoF$_4$ single crystal were measured using a SQUID magnetometer, and the angular dependences of the magnetization were obtained by the inductive method. As follows from the calculations, the significant anisotropy of the magnetization is mainly due to the magnetoelastic interaction, which makes a relatively large contribution to the magnitude of the magnetization at temperatures less than 10 K and in fields $B > 0.5$ T.

When calculating the magnetization along the crystallographic axis a, an error was taken into account in the orientation of the single crystal (due to the small ball diameter of 2 mm), which was 6° in the ac plane of the crystal lattice. Figure 15 shows the angular dependence of the magnetization of a single crystal of LiHoF$_4$ in the basal plane. It is seen that the magnetization anisotropy is almost absent. The contribution of the electron-phonon interaction is not significant and was not taken into account during the calculation. The anisotropy of
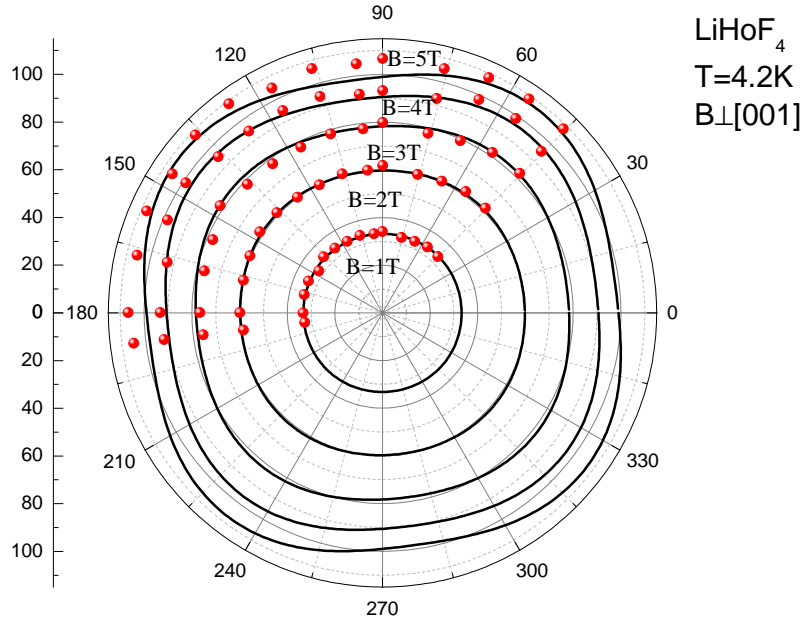
Figure 15. Angular dependences of the magnetization in the basis plane of $LiHoF_4$ single crystal at $T = 4.2$ K. Solid lines correspond to the results of calculations, symbols correspond to experimental data.

magnetization in the basal plane is very weakly expressed and the magnetoelastic interaction is much weaker than in $LiTmF_4$ and $LiDyF_4$, which is confirmed by the large magnitude of magnetostriction in these single crystals.

The parameters of the crystal field in a single crystal of $LiHoF_4$ and the parameters of the electron-deformation interaction are determined from an analysis of the obtained data and calculations of the magnetization taken into account with the electron-deformation interaction. A self-consistent description of magnetization, the field dependences of magnetostriction in different directions of the applied magnetic field is presented.

9. Magnetic and magnetoelastic properties of $LiDyF_4$ single crystals

A $LiDyF_4$ single crystal is a dipole XY antiferromagnet with magnetic moments of Dy^{3+} ions directed perpendicular to the axis of the crystal lattice [7]. An analysis of the magnetic dipole and exchange interactions between the Dy^{3+} ions and the magnetic structure was carried out on the basis of measurements of the low-temperature heat capacity in [31]. The effects caused by the intersection of the energy levels of the Dy^{3+} ion in a $LiDyF_4$ single crystal in strong pulsed magnetic fields were also investigated previously [32]. In this work, the magnetization of a $LiDyF_4$ single crystal is calculated. The magnetic dipole interaction between the Dy^{3+} ions was taken into account by the introduction of a local magnetic field Eq. 26. The crystal field on the Dy^{3+} ion in a $LiDyF_4$ single crystal in the crystallographic coordinate system is determined by a set of 7 parameters (Table 9).

The values of the parameters of the electron-deformation interaction used in this work are listed in Table 10. The parameters of multipole interactions are given in Table 11.

The results presented below were obtained using the numerical diagonalization of the Hamiltonian of the Dy^{3+} ions in the complete state basis of the $4f^9$ electron configuration (the number of states is 2002). The free ion Hamiltonian is written in the standard form with the parameters of electrostatic, spin-orbit and interconfiguration interactions taken from [8]. The calculated magnetization behaviour in an external magnetic field rotating around an arbitrary axis is shown

Table 9. Crystal field parameters B_p^k (cm^{-1}), acting on Dy^{3+} in LiDyF$_4$ single crystals.

			Dy^{3+} $(4f^9)$ $^6H_{15/2}$		
p	k	[32]	[4]	[12]	This work
2	0	182	170	165	160±3
4	0	−53	−85	−88	−83±3
6	0	1.5	−4.2	−4.4	−4.6±0.2
4	4	−806	−721	−980	−751±5
4	−4	−380	−661	0	−641±5
6	4	−654	−390	−427	−360±5
6	−4	−272	−248	−65	−243±5

Table 10. Interaction parameters between Dy^{3+} ions and lattice deformations of B_g symmetry in a LiDyF$_4$ single crystal (cm^{-1}). The effective parameters are given for a zero magnetic field and a temperature $T = 4.2$ K.

p k	2 2	2 −2	4 2	4 −2	6 2	6 −2	6 6	6 −6
$\hat{B}_p^k(B_g^1)$	1997	2355	−887	1200	−135	−427	−731	−691
$B_{\text{eff}}{}_p^k(B_g^1)$	1617	3817	−1497	1766	−322	−549	−614	−1022
$\hat{B}_p^k(B_g^2)$	4114	−1144	−1120	1652	−528	−375	−841	−878
$B_{\text{eff}}{}_p^k(B_g^2)$	4614	−4406	337	168	−126	−4	−997	−98

Table 11. Parameters of the multipole interaction λ_{ij} (cm^{-1}) in a LiDyF$_4$ crystal.

i/j	1	2	3	4	5	6	7	8
1	−72	−54.8	48.49	−54.8	10.18	26.5	22.5	29.96
2		62.98	−17.8	10.88	−7.13	3.516	16.07	−6.56
3			−2.0	4.572	−3.15	−0.48	−13.6	−4.88
4				−28.6	−1.77	4.771	14.09	1.137
5					−1.94	−1.16	−4.15	−1.7
6						−1.93	−5.53	−6.8
7							−6.56	−9.05
8								−6.29

in Figure 16. The direction of the axis of rotation was determined by the angle θ between the axis of rotation and the crystallographic axis c and the angle α between the projection of the axis of rotation to the ab plane of the crystal and axis θ. It can be seen that a small deviation of the external magnetic field from the crystallographic axes of the crystal leads to significant distortions of the angular dependence of the magnetization in the basal ab plane of the lattice.

The temperature and magnetic field dependences of the magnetization of a LiDyF$_4$ single crystal were measured using SQUID magnetometer. The experimental data are well described by a theoretical model, within which interionic multipole interactions are taken into account.
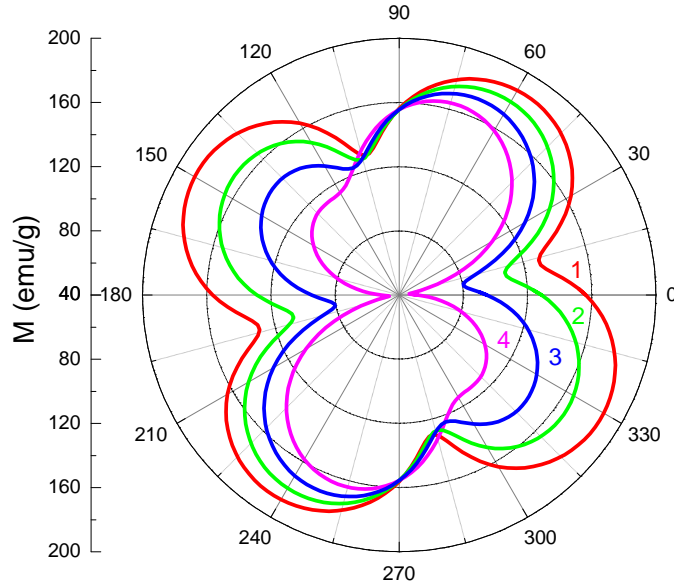
Figure 16. The calculated angular dependence LiDyF$_4$ single crystal magnetization in an external magnetic field in different planes ($B = 2$ T) : $1 - \theta = 0, \alpha = 0$; $2 - \theta = 5°, \alpha = 30°$; $3 - \theta = 5°, \alpha = 45°$; $4 - \theta = 5°, \alpha = 60°$ [7].

The results of magnetization calculations using the set of proposed parameters of the crystal field and with the renormalized coupling constants between macro and micro deformations are shown in Figures 17, 18.

The observed non-monotonic behaviour of magnetization at low temperatures with a maximum close to 25 K and a minimum of about 5 K (see Figure 17a) is explained by the specific relationship between the corresponding components of the g-tensor of the main ($g_\parallel = 1.15$) and first excited ($g_\parallel = 5.3$) the sublevel of the $^6H_{15/2}$ multiplet of the Dy^{3+} ion in the crystal field, and also taking into account the redistribution of the occupations of the Kramers doublets with a change in temperature. From the comparison of the calculated and measured temperature dependences of the magnetization in the field $\mathbf{B} \parallel c$ (see Figure 17), we clarified the values of the parameters of the crystal field (see Table 9). We note that the calculated energy of 18.6 cm^{-1} of the first excited sublevel of the main $^6H_{15/2}$ multiplet differs noticeably from the corresponding energy of 14.2 cm^{-1} of Dy^{3+} ions in a LiYF$_4$ crystal [22]. We determined the parameters of the crystal field and compared with the literature data in Table 9. The significant role of electron-deformation interaction in the formation of magnetization in concentrated rare-earth paramagnets at low temperatures becomes evident when we analyze the magnetization of LiDyF$_4$ induced by a magnetic field perpendicular to the c axis (Figure 18). In this case, as shown in Fig. 18b, taking into account only the Zeeman interaction, we observe highly underestimated magnetic moments of the Dy^{3+} ion in fields exceeding 1 T.

It should be noted that the multipole interaction introduces a noticeable renormalization to the electron-deformation interaction, and one can expect a strong softening of the LiDyF$_4$ crystal lattice, similar to that observed in DyVO$_4$ [32]. The calculated temperature dependences of the elastic constants LiDyF$_4$, which are determined by the induced B_g symmetry deformations, are shown in Fig. 19. In fact, the elastic constants change significantly with decreasing temperature to 10 K and subsequently remain unchanged at low temperatures.

At low temperatures a giant magnetostriction is induced in a magnetic field ~ 1 T in a LiDyF$_4$ single crystal at $T = 4.2$ K. The calculated changes in the crystal size along the direction of
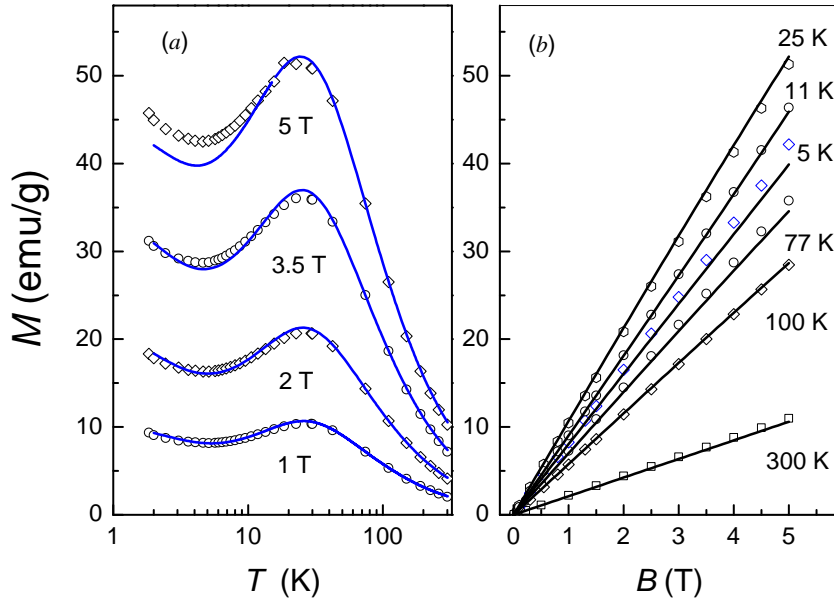
Figure 17. Measured (symbols) and calculated (solid lines) temperature (a) and field (b) dependences of the magnetization in LiDyF$_4$ for different values of the magnetic field ($\mathbf{B} \parallel c$) and temperature [7].
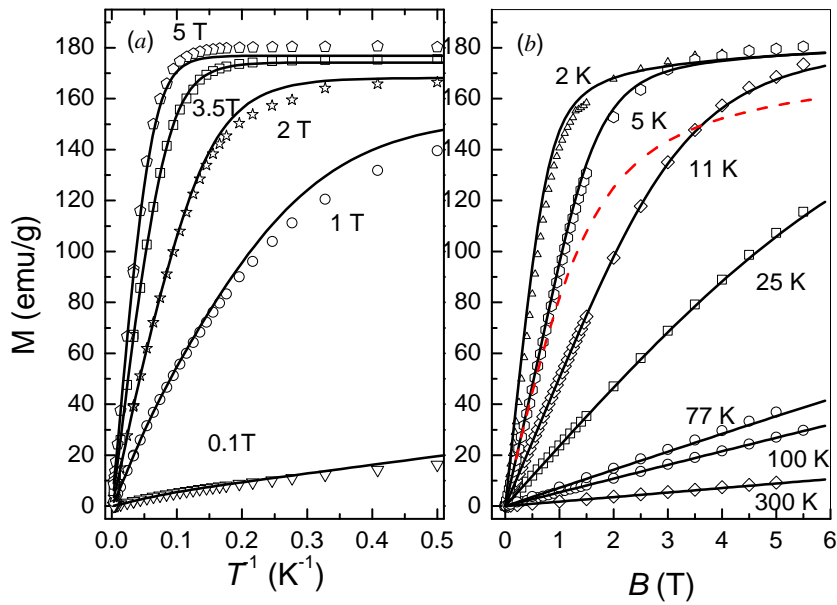

Figure 18. Magnetic fields dependences (solid lines – calculations, symbols – experiment) of the magnetization in LiDyF$_4$ in a magnetic field. The dashed curve shows the calculated magnetization at $T = 5$ K without taking into account the electron-deformation interaction [7].

the external magnetic field given by the guide cosines $\Delta l/l = \sum_{\alpha\beta} n_\alpha n_\beta e_{\alpha\beta}$, using the above parameters of the crystal field, are in good agreement with the measurement data (see Figure 20) when taking into account temperature and magnetic field-dependent contributions to elastic constants due to the electron-deformation interaction.

The temperature and field dependences of the magnetization and field dependences of the strongly anisotropic magnetostriction in LiDyF$_4$ single crystals were measured. The giant magnetostriction of $\approx 10^{-3}$ was observed in a rather small magnetic field of 1 T directed along the [110] crystallographic axis at liquid helium temperature. The sets of parameters which define interactions of the Dy^{3+} ions with the crystal field and the crystal lattice uniform deformations

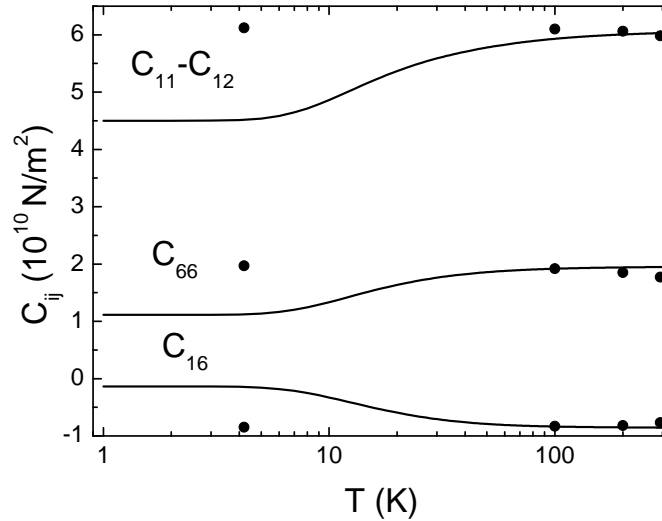*Magnetic Resonance in Solids. Electronic Journal. 2019, Vol. 21, No 4, 19412 (26 pp.)*

23

Figure 19. Calculated temperature dependences of elastic constants in a zero magnetic field. The values of the corresponding elastic constants of the $LiYF_4$ single crystal are shown by the symbols [7, 33].
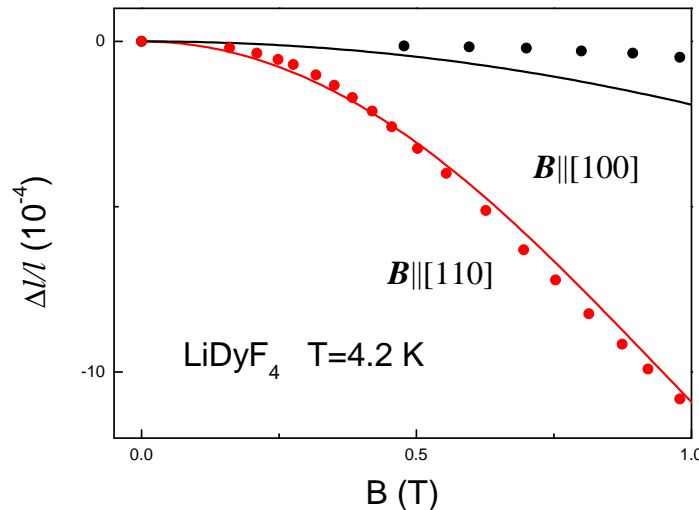

Figure 20. Field dependence of the magnetostriction in the two directions of the applied magnetic field in $LiDyF_4$ single crystal at $T = 4.2$ K. The solid lines – the theory, symbols – experimental data [7].

as well as the parameters of the multipole interactions between the Dy^{3+} ions were determined. The results of the measurements are well reproduced by simulations. The magnetoelastic interaction in $LiDyF_4$ contributes essentially to the magnetization in external magnetic fields oriented in the basis plane of the crystal lattice at low temperatures.

10. Conclusion

We have measured and calculated elastic, spectral, and magnetic characteristics of a single crystals $LiLnF_4$ taking into account the electron-deformation and multipole interactions. It has been shown that the entire set of experimental data available at present time on the field and temperature dependences of elastic constants, magnetization, magnetostriction, and energy levels can be reproduced not only qualitatively, but also quantitatively, with a satisfactory accuracy in terms of a self consistent theory that uses a unified set of parameters of the crystal field and electron-deformation and multipole interactions.

Acknowledgments

References

1. Boldyrev K.N., Popova M.N., Malkin B.Z., Abishev M.N. *Phys. Rev. B* **99**, 041105 (2019)

2. Dunn J.L., Stahl C., Macdonald A.J., Liu K., Reshitnyk Y., Sim W., Hill R.W. *Phys. Rev. B* **86**, 094428 (2012)

3. Vasyliev V., Villora E. G., Nakamura M., Sugahara Y., Shimamura K. *Opt. Express* **20**, 14460 (2012)

4. Aminov L.K., Malkin B.Z., Teplov M.A. *Handbook on the Physics and Chemistry of Rare Earths* **22**, 295 (1996)

5. Rønnow H., Jensen J., Parthasarathy R., Aeppli G., Rosenbaum T.F., McMorrow D.F., Kraemer C.W. *Phys. Rev. B* **75**, 054426 (2007)

6. Al'tshuler S.A., Krotov V.I., Malkin B.Z. *JETP Lett.* **32**, 214 (1980)

7. Romanova I.V., Korableva S.L., Krotov V.I., Malkin B.Z., Mukhamedshin I.R., Suzuki H., Tagirov M.S. *J. Phys.: Conf. Ser.* **478**, 012026 (2013)

8. Romanova I.V., Malkin B.Z., Tagirov M.S. *Opt. Spectrosc.* **116**, 897 (2014)

9. Aminov L.K., Malkin B.Z. *Dynamics and Kinetics of Electronic and Spin Excitations in Paramagnetic Crystals*, Kazan State University, Kazan (2008) (*in Russian*)

10. Eyring L., Gschneidner K.A., Lander G.H. *Handbook on the Physics and Chemistry of Rare Earths* **32** (2002)

11. Christensen H.P. *Phys. Rev. B* **19**, 6573 (1979)

12. Kupchikov A.K., Malkin B.Z., Rzaev D.A., Ryskin A.I. *Fizika Tverdogo Tela* **24**, 2373 (1982) (*in Russian*)

13. Klimin S.A., Pytalev D.S., Popova M.N., Malkin B.Z., Vanyunin M.V., Korableva S.L. *Phys. Rev. B* **81**, 045113 (2010)

14. Abubakirov D.I., Matsumoto K., Suzuki H., Tagirov M.S. *J. Phys.: Cond. Mat.* **20**, 395223 (2008)

15. Abdulsabirov R.Y., Kazantsev A.A., Korableva S.L., Malkin B.Z., Nikitin S.I., Stolov A.L., Tagirov M.S., Tayurskii D.A., van Tol J. *XI Feofilov Symposium on Spectroscopy of Crystals Activated by Rare-Earth and Transition Metal Ions* **4766**, 59 (2002)

16. Al'tshuler S.A., Malkin B.Z., Teplov M.A., Terpilovskii D.N. *Sov. Sci. Rev.: Sect. A* **6**, 61 (1985)

17. Abdulsabirov R.Y., Kazantsev A.A., Korableva S.L., Malkin B.Z., Nikitin S.I., Stolov A.L. *J. Lumin.* **117**, 225 (2006)

18. Abubakirov D.I., Kuzmin V.V., Suzuki H., Tagirov M.S., Tayurskii D.A. *J. Phys.: Conf. Ser.* **51**, 135 (2006)

19. Romanova I.V., Malkin B.Z., Mukhamedshin I.R., Suzuki H., Tagirov M.S. *Phys. Solid State* **44**, 1544 (2002)

20. Hansen P.E., Nevald R. *Phys. Rev. B* **16**, 146 (1977)

21. Christensen H.P. *Phys. Rev. B* **17**, 4060 (1978)

22. Nevald R., Hansen P.E. *Physica B+C* **86**, 1443 (1977)

23. Liu G., Jacquier B. *Spectroscopic Properties of Rare Earths in Optical Materials* **83**, 1443 (Springer Science and Business Media, 2006)

24. Bumagina L.A., Krotov V.I., Malkin B.Z., Khasanov A.K. *Zh. Eksp. Teor. Fiz* **80**, 1543 (1981) (*in Russian*)

25. Kjaer K., Als-Nielsen J., Laursen I., Larsen F.K. *J. Phys.: Cond. Mat.* **1**, 5743 (1989)

26. Kazei Z.A., Snegirev V.V., Broto J.M., Abdulsabirov R.Y., Korableva S.L. *J. Exp. Theor. Phys.* **115**, 1029 (2012)

27. Romanova I.V., Abdulsabirov R.Y., Korableva S.L., Malkin B.Z., Mukhamedshin I.R., Suzuki H., Tagirov M.S. *Magn. Reson. Solids* **8**, 1 (2006)

28. Shakurov G.S., Vanyunin M.V., Malkin B.Z., Barbara B., Abdulsabirov R.Y., Korableva S.L. *Appl. Magn. Res.* **28**, 251 (2005)

29. Christensen H.P. *Phys. Rev. B* **19**, 6564 (1979)

30. Romanova I.V., Klochkov A.V., Korableva S.L., Kuzmin V.V., Malkin B.Z., Mukhamedshin I.R., Suzuki H., Tagirov M.S. *Magn. Reson. Solids* **14**, 12203 (2012)

31. Beauvillain P., Chappert C., Renard J.P., Griffin J.A., Laursen I. *J. Magn. Magn. Mat.* **15**, 421 (1980)

32. Kazei Z.A., Snegirev V.V., Chanieva R.I., Abdulsabirov R.Y., Korableva S.L. *Phys. Solid State* **48**, 726 (2006)

33. Blanchfield P., Saunders G.A. *J. Phys. C: Solid State Phys.* **12**, 4673 (1979)